Available online at www.sciencedirect.com
SCIENCE DIRECT®
PERGAMON
Polyhedron 22 (2003) 2527–2535
POLYHEDRON
www.elsevier.com/locate/poly

A pseudo-Jahn–Teller model of the photochromic effect in sodium nitroprusside

E. Coronado [a], S. Klokishner [b,*], O. Reu [b], B. Tsukerblat [c]

[a] Instituto de Ciencia Molecular, Universitat de València, Dr Moliner 50, 46100 Burjassot, Spain
[b] State University of Moldova, Mateevich Street 60, Kishinev 2009, Moldova
[c] Ben-Gurion University of the Negev, Beer-Sheva 84105, Israel

Received 20 November 2002; accepted 4 February 2003

Abstract

A new model for the photochromic effect in sodium nitroprusside $Na_2[Fe(CN)_5(NO)]\cdot 2H_2O$ based on the concept of the pseudo-Jahn–Teller effect is proposed. The model takes into account the electron transfer from the Fe^{2+} ion to the π^* orbitals of the NO-ligand as well as the vibronic mixing of three electronic states of the Fe–NO fragment through the non-symmetric and full-symmetric modes. The problem is solved within the adiabatic approximation. Under certain conditions the lower sheet of the adiabatic potential is shown to possess three minima with the increasing energies that correspond to the N-bound, sideways bound and O-bound NO group. The barriers between the minima are estimated and the excited minima are attributed to the MS2 and MS1 metastable states observed experimentally.

Keywords: Photochromic effect; Metastable states; Pseudo-Jahn–Teller effect; Electron transfer

1. Introduction

A fascinating phenomena of the photochromic effect has been discovered in several nitrosyl complexes of transition metal ions [1–6]. At low temperatures the most extensively studied sodium nitroprusside $Na_2[Fe(CN)_5(NO)]\cdot 2H_2O$ (SNP) demonstrates two excited metastable states (MS1 and MS2) induced by the visible light in the region 350–600 nm. At temperatures below 150 K the metastable states are extremely long-living and do not show any indications of spontaneous and thermal decay. Both metastable states can be depopulated by temperature rise or reversibly converted back to the ground state (GS) by red light irradiation. During the thermal decay of the metastable states no emission of radiation could be observed in the energy range 0.3–5 eV. Calorimetry experiments [7] show that the MS1 state is higher in energy than the MS2 state. Above 160 K the decay of the metastable states of SNP obey the Arrhenius law with the activation energies 0.7 and 0.5 eV for MS1 and MS2 [8]. The change in color exhibited with the generation of the excited MS1 and MS2 states has been proposed as the basis for the information storage system, since information can be written and erased reversibly using the light of two different wavelengths [8]. An essential advance in the study of the photochromic effect came from X-ray diffraction experiments [9,10] with the aid of which the geometries of the ground and the two excited metastable states have been determined. The Fe–(NO) group was found to be linear in the GS. The diffraction evidences a bent geometry of the system in MS2 state in which NO is sideways bound, while in the MS1 state an interchange of N and O takes place so that the NO group is connected with Fe through oxygen. Mössbauer [11] and electron-spin resonance measurements [12] proved that the GS and both metastable states are diamagnetic. The downshift of NO stretch and Fe–(NO) stretch frequencies suggest weaker bonds for MS1 and MS2 [13].

* Corresponding author. Fax: +373-2-738149.
E-mail addresses: eugenio.coronado@uv.es (E. Coronado), klokishner@yahoo.com (S. Klokishner), tsuker@bgumail.bgu.ac.il (B. Tsukerblat).

0277-5387/03/$ - see front matter
doi:10.1016/S0277-5387(03)00172-4

Metastable states with similar properties have been found in several nitrosyl–ruthenium and nitrosyl–osmium complexes [3–6].

Previous theoretical studies were focused on the DFT calculations of the energy of the SNP [14–16] as a function of the angle ∠FeNO. In [14–16] it was revealed that three minima of the ground term correspond to three possible configurations of the Fe–NO fragment: linear, bent and inverted. At the same time DFT calculations [14–16] give a correct order of the energies of the GS, MS1 and MS2 states. In the ab initio calculations carried out in forthcoming paper [17] the number of the variable structural parameters is extended and along with the consideration of the ground potential surface of the SNP the consideration in [17] takes into account the transition states connecting the states GS with MS2 and MS2 with MS1 that makes clear the effect of the transition states on the photo-isomerisation.

Here we suggest a new model of the phenomenon based on the concept of the pseudo-Jahn–Teller (PJT) effect. As distinguished from the previous work our vibronic model allows us to examine the physical origin of the nuclear rearrangement and the underlying mechanism of the photochromic effect at the electronic level. At the same time the proposed approach can be considered as a background for the dynamical (quantum-mechanical solution) of the problem of light absorption and emission including the crucial question of interpretation of the anomalous lifetimes for the excited states and band-shapes of the optical bands.

2. The model

At the first step we consider the FeNO fragment of the whole SNP that is really involved in the photochromic reorganization. This approximation enables us to simplify the problem and to give clear insight on the mechanism of the phenomenon. Following the idea of the PJT effect we start with the 'reference' configuration of the FeNO fragment that is chosen to be triangular and its symmetry is supposed to be C_{2V}. The electronic basis includes the states of the system with the following fixed oxidation degrees of the fragments: $^1A_1(Fe^{2+}(d^6))$, $^1A_2(Fe^{3+}(d^5)\pi_x^*NO)$, $^1B_2(Fe^{3+}(d^5)\pi_y^*NO)$ (Fig. 1). This states are connected by the electron transfer from the Fe^{2+} -ion to the π* level of the NO ligand, here A_1, A_2, B_2 are the irreducible representations of the C_{2V} group. The PJT problem arises from the mixing of the $^1A_2$ and $^1B_2$ states by the B_1-vibration of the triangle. The coupling of the states $^1A_1$, $^1A_2$, $^1B_2$ through the full-symmetric vibration of the FeNO fragment is taken into account as well. In such a way we face a two-mode-three level PJT problem $(A_1+A_2+B_2)\otimes(A_1+B_1)$. The normal vibrational modes B_1 and A_1 of the FeNO fragment are shown in Fig. 2.

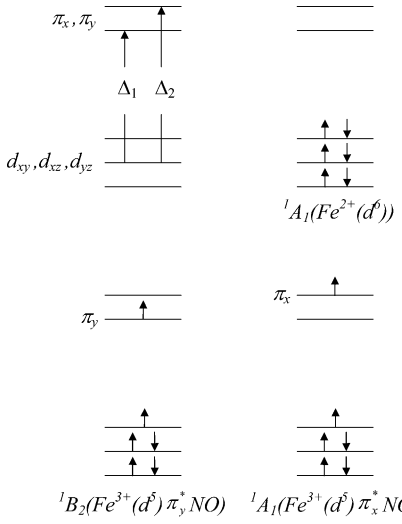

Fig. 1. Scheme of the electronic states of the Fe–(NO) fragment.

The full Hamiltonian of the fragment is presented in the form

$$H = H_e + H_{eL} + H_L \tag{1}$$

Here H_e is the electronic Hamiltonian determining the wave functions and the eigenvalues of the Fe–(NO) fragment in the fixed nuclear configuration. Reading off the coordinate q_{A_1} of the full-symmetric vibration from its equilibrium position in the state $^1A_1(Fe^{2+}(d^6))$, one can write down the operator of the linear electron-vibrational interaction in the following form:

$$\begin{aligned} H_{eL} &= (v_{A_1}(\mathbf{r}) - v)(q_{A_1} - q^o_{A_1}) + V_{B_1}(\mathbf{r})Q \\ &\equiv V_{A_1}(\mathbf{r})q + V_{B_1}(\mathbf{r})Q \end{aligned} \tag{2}$$

here $\mathbf{r}$ represents the set of electronic coordinates of the Fe–(NO) fragment, $v = \langle {}^1A_1|v\,A_1(\mathbf{r})|{}^1A_1\rangle$, $q^o_{A_1} = -v/\hbar\omega_{A_1}$, ω_{A_1} is the vibrational frequency of the full-symmetric mode, $q = q_{A_1} - q^o_{A_1}$, the second term in Eq. (2) describes the operator of interaction with the B_1-mode. Finally, H_L is the Hamiltonian of free lattice vibrations

$$H_L = \frac{\hbar\omega_{A_1}}{2}\left(q^2 - \frac{\partial^2}{\partial q^2}\right) + \frac{\hbar\omega_{B_1}}{2}\left(Q^2 - \frac{\partial^2}{\partial Q^2}\right) \tag{3}$$

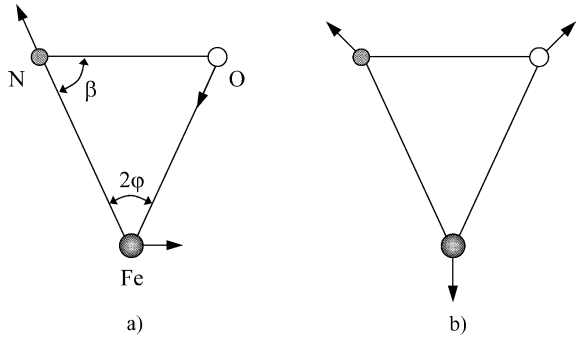

Fig. 2. Vibrations of the Fe–(NO) fragment: a, non-symmetric $_{B_1}$-vibration; b, full-symmetric A_1-vibration.

where ω_{B_1} is the vibrational frequency of the B_1 mode. Solving the classical problem of the normal vibrations we obtain the following expressions for the frequencies ω_{B_1} and ω_{A_1}:

$$\omega_{B_1} = \left(\frac{k}{m}\left(1+\frac{2m}{M}\sin^2(\varphi)\right)\right)^{1/2} \tag{4}$$

$$\omega_{A_1} = \left(\frac{k}{2mM} \times (3(m+M) - M\cos(2\varphi) - [(M\cos(2\varphi) - 3(m+M))^2 - 8m(m+2M)]^{1/2})\right)^{1/2}$$

where k is the mean force constant, m is the mass of Fe ion, M is the mean mass of N and O atoms, 2φ is the N–Fe–O—angle in the 'reference' configuration (Fig. 2). For the sake of simplicity the second full-symmetric vibration of the triangular Fe–(NO) moiety will not be taken into account insofar as the effect of both full-symmetric vibrations is similar.

The non-diagonal matrix elements $\langle {}^1A_1|H_e|{}^1A_1\rangle$ and $\langle {}^1B_1|H_e|{}^1A_1\rangle$ of the electronic Hamiltonian H_e represent parameters describing the electron transfer from the Fe^{2+}-ion to the π* level of the NO ligand. At the first step these parameters were put equal to $\langle {}^1A_1|H_e|{}^1A_1\rangle = \langle {}^1B_1|H_e|{}^1A_1\rangle = t$. In the model under consideration three vibronic parameters are involved. The parameter $V = \langle {}^1A_1|V_{B1}|{}^1B_1\rangle$ characterizes the coupling of the states ${}^1A_2(Fe^{3+}(d^5)\pi_x^*NO)$ and ${}^1B_2(Fe^{3+}(d^5)\pi_y^*NO)$ by the B_1-mode. The parameters $\upsilon_1\langle {}^1B_1|\upsilon_{A1}|{}^1B_1\rangle - \upsilon$ and $\upsilon_2\langle {}^1A_1|\upsilon_{A1}|{}^1A_1\rangle - \upsilon$ describe the interaction of the states ${}^1B_2$ and ${}^1A_2$ with the full-symmetric A_1-mode. The matrix of the Hamiltonian H in the basis of the states ${}^1A_2$, ${}^1B_2$, ${}^1A_1$ can be represented in the following form:

$$H = \begin{pmatrix} \Delta_2 + \upsilon_2 q & VQ & t \\ VQ & \Delta_1 + \upsilon_1 q & t \\ t & t & 0 \end{pmatrix} + H_L\hat{I} \tag{5}$$

where $\hat{I}$ is the unit 3×3-matrix. Then we employ the adiabatic approximation, neglecting thus the nuclear kinetic energy in the Hamiltonian H_L, Eq. (3). In this approximation the energies of the Fe–(NO) fragment represent the adiabatic potentials. The analytical expression for the adiabatic potential is cumbersome and for this reason this expression is not given here.

3. Ground adiabatic potential sheet

The shapes of the adiabatic potential sheets are governed by eight parameters V, υ_1, υ_2, Δ_1, Δ_2, t, ω_{B_1}, ω_{A_1}. In order to elucidate the conditions which favor the photochromic effect, first we shall try to discuss the values of the above-mentioned parameters. For the usually accepted value of $k \approx 10^5$ dyn cm^{-1} the frequencies ω_{B_1} and ω_{A_1} are estimated as 344 and 403 cm^{-1}, respectively. The energy gaps Δ_2 and Δ_1 can be approximately identified with those between the HOMO and the split components of LUMO in the MS2 state. These values are calculated in paper [17] by the DFT method and prove to be equal to $\Delta_2 = 21\,185$ cm^{-1} and $\Delta_1 = 15\,850$ cm^{-1}. The vibronic coupling parameter V was roughly estimated with the aid of assumption that $\upsilon_1 = \upsilon_2 = 0$, $t = 0$. In this case from Eq. (5) a simple analytical expressions for the sheets of the adiabatic potential can be found:

$$u_1(Q) = \frac{\hbar\omega_{B_1}Q^2}{2} \tag{6}$$

$$u_{2,3}(Q) = \frac{\hbar\omega_{B_1}Q^2}{2} + \frac{\Delta_1+\Delta_2}{2} \mp \frac{\sqrt{(\Delta_1-\Delta_2)^2 + 4V^2Q^2}}{2}$$

The ground adiabatic potential sheet $u_2(Q)$ has two equivalent minima at the points:

$$Q'_{1,3} = \pm\frac{1}{2V}\left(\left(\frac{2V^2}{\hbar\omega_{B_1}}\right) - (\Delta_2-\Delta_1)^2\right)^{1/2} \tag{7}$$

while the sheets $u_1(Q)$ and $u_3(Q)$ possess one minimum at the point $Q'_2 = 0$. If the energy

$$E_a = \frac{\hbar\omega_{B_1}}{8V^2}(\Delta_2+\Delta_1)^2 + \frac{V^2}{2\hbar\omega_{B_1}} - \frac{\Delta_1+\Delta_2}{2} \tag{8}$$

of the thermally activated transition from the sheet $u_2(Q)$ to the sheet $u_1(Q)$ is set to be equal to the value 0.5 eV estimated by the calorimetry methods [7] for the MS2 state, one can estimate the parameter V as $V = 9.65\omega_{B_1}$. The validity of this evaluation will be discussed below. The parameter t was taken in the range $0 \le t \le 10\omega_{B_1}$. Insofar as the energy gap Δ_2 exceeds significantly the gap Δ_1 the parameter υ_2 was taken bigger than the parameter υ_1. Such a relation is predicted by the crystal field theory [18]. In Fig. 3 two different side views of the ground adiabatic potential sheet are shown for the set of parameters $V = 9.8\hbar\omega_{B_1}$, $t = 5.5\hbar\omega_{B_1}$, $\upsilon_2 = 6.2\hbar\omega_{B_1}$, $\upsilon_1 = 1.5\hbar\omega_{B_1}$, $\Delta_1 = 15\,850$ cm^{-1}, $\Delta_2 = 21\,185$ cm^{-1}, $\omega_{B_1} = 344$ cm^{-1}, $\omega_{A_1} = 403$ cm^{-1}. From Fig. 3a it is seen that the lower adiabatic potential branch has three minima, the energies of these minima successively increase, so that the energy of the ground minimum is $-1.93\hbar\omega_{B_1}$, whereas the energies of the excited minima are equal to $-1.15\hbar\omega_{B_1}$ and $-0.84\hbar\omega_{B_1}$. In such a way, at temperatures below 180 K the thermal population of both excited minima is negligible. The order of minima alternation is also confirmed by Fig. 4 illustrating the contour plot. At the same time Fig. 3(a) clearly demonstrates that the potential barrier separating the ground and first excited minima is lower than that separating the excited minima. A quantitative estima-

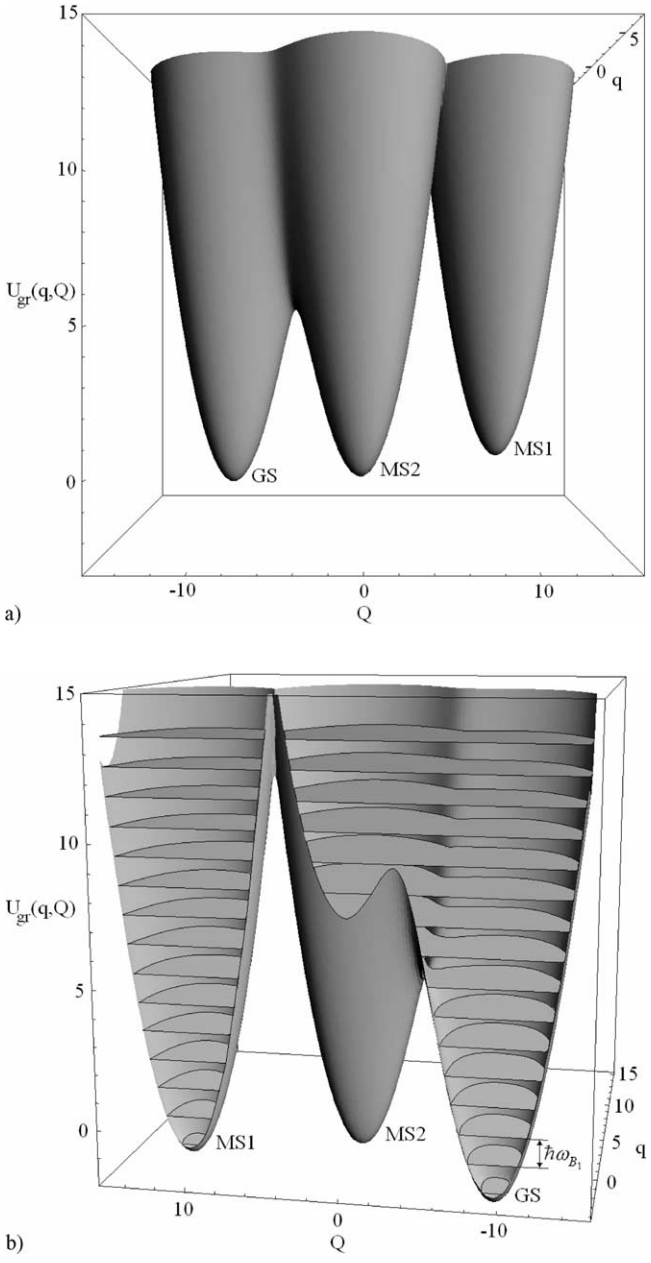

Fig. 3. Different views of the lower adiabatic potential sheet $U_{gr}(q,Q)$ in the case of $V = 9.8\hbar\omega_{B_1}$, $t = 5.5\hbar\omega_{B_1}$, $\upsilon_2 = 6.2\hbar\omega_{B_1}$, $\upsilon_1 = 1.5\hbar\omega_{B_1}$, $\Delta_1 = 15\,850\ \mathrm{cm}^{-1}$, $\Delta_2 = 21\,185\ \mathrm{cm}^{-1}$, $\omega_{B_1} = 344\ \mathrm{cm}^{-1}$, $\omega_{A_1} = 403\ \mathrm{cm}^{-1}$.

tion of the barrier heights can be made with the aid of Fig. 3(b) wherein the adiabatic potential wells are cut by horizontal planes separated by the gaps $\hbar\omega_{B_1}$. The height of the barrier between the ground and the first excited minima is about $7.3\hbar\omega_{B_1} \approx 0.3$ eV. The barrier between the first and the second excited minima attains the value $13.7\hbar\omega_{B_1} \approx 0.6$ eV. At the next stage we determine the geometrical structure of the Fe–(NO) cluster corresponding to the minima of the ground adiabatic potential surface. With allowance for the relations between the Cartesian displacements of the Fe, N and O atoms and the normal vibrational coordinates q and Q [19,20] of the FeNO fragment the angle $\beta \angle$ FeNO (Fig. 2) can be expressed as a function of the coordinates $\tilde{Q}_i$ and $\tilde{q}_i$ of the minima of the ground adiabatic potential sheet:

$$\begin{aligned}\beta_i = {} & \frac{\pi}{2} - \mathrm{Arc}\,\sin[\tilde{Q}_i\sqrt{m}\sqrt{M+m-m\cos(2\varphi)}\,\cot(\varphi)/ \\ & (l\sqrt{2M}(\sqrt{M}+\sqrt{m}-\sqrt{M}\cos(2\varphi)))] \\ & -\mathrm{Arc}\,\sin[\sin(\varphi)+\tilde{Q}_i\sqrt{M} \\ & \sqrt{2M+4m\sin^2(\varphi)}\,\sin(\varphi)\cos^2(\varphi)/ \\ & (l(m+2\sqrt{Mm}\sin^2(\varphi))) \\ & +(\tilde{q}_i\sin(2\varphi)(2M+m) \\ & \times(\sqrt{2M+4m} \\ & \times(3M-\sqrt{(M\cos(2\varphi)-3(M+m))^2-8m(2M+m)}) \\ & +\sqrt{2}\sqrt{M+2m}(m-M\cos(2\varphi))))/ \\ & (4l\sqrt{Mm}(2\sqrt{M}+\sqrt{m})((M+m)\cos(2\varphi) \\ & -3M+\sqrt{(M\cos(2\varphi))-3(M+m)^2-8m(2M+m)}))]\end{aligned} \tag{9}$$

here l is the mean distance between Fe and N or between Fe and O atoms in the 'reference' configuration (Fig. 2), the indices $i = 1$–3 label the dimensional coordinates $\tilde{q}_i$, $\tilde{Q}_i$ and the angle β_i corresponding to the ground, first and second excited minima of the lower adiabatic potential branch. The values $\tilde{Q}_i$ and $\tilde{q}_i$ are connected with the dimensionless coordinates Q_i and q_i that appear in Eqs. (2) and (3) by the relations:

$$\tilde{Q}_i = Q_i\sqrt{\hbar/M_{B_1}\omega_{B_1}}, \quad \tilde{q}_i = q_i\sqrt{\hbar/M_{A_1}\omega_{A_1}} \tag{10}$$

where M_{B_1} and M_{A_1} are the effective masses for the B_1- and A_1-vibrations [19,20]. The numerical values of M_{B_1} and M_{A_1} are equal to 3.545×10^{-23} g and 1.15×10^{-22} g, correspondingly. In the Table 1 the calculated values of the angle β_i corresponding to the lowest (β_1) and the excited minima (β_2, β_3) of the ground adiabatic potential sheet are given together with the experimental values of these angles determined by X-ray diffraction studies [10]. The angles β_i were evaluated with the values $l = 1.95 \times 10^{-8}\ \mathrm{cm}^{-1}$ and $\varphi = 16.5^\circ$ taken from [10]. In the Table 1 the dimensionless coordinates Q_i and q_i of the adiabatic potential minima are also listed. For the chosen set of parameters the obtained values of the angles β_i are in quite a good agreement with experimental data [10]. So, the lowest minimum corresponds to the usual bonding of the Fe-ion with the NO-group and can be identified with the GS. The first excited minimum describes the bent geometry and can be assigned to the MS2 state. The highest minimum relates to a linear configuration, in which the NO-ligand has rotated by about 180° compared to the GS. Such an arrangement of the NO-group is characteristic of the MS1 state.

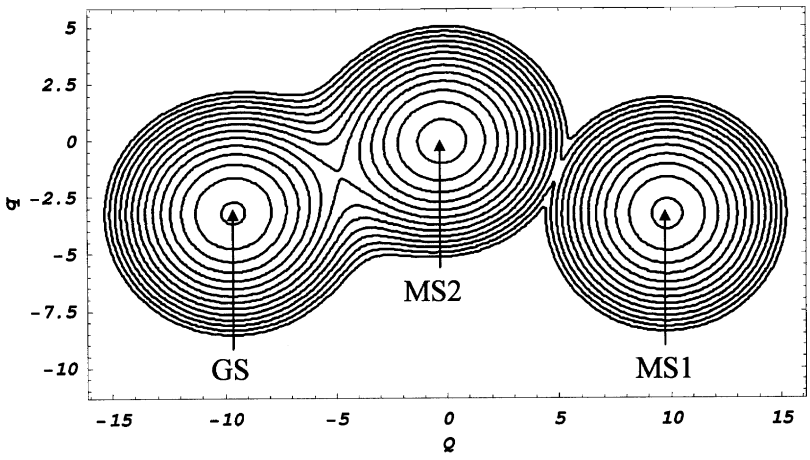

Fig. 4. Contour plot of the lower sheet $U_{gr}(q,Q)$. The parameters are the same as in Fig. 3.

It should be mentioned that the coordinates Q_1 and Q_3 (see the Table 1) of the ground and second excited minima nearly coincide with those estimated for $V = 9.8\hbar\omega_{B_1}$ with the aid of Eq. (7). At the same time the coordinate Q_2 of the first excited minimum is close to zero. From this it follows that the minima of the sheet $u_2(Q)$ (Eqs. (6) and (7)) convert into the minima GS and MS1 at the points Q_1 and Q_3 given in the Table 1, whereas the minimum of the sheet $u_1(Q)$ turns into the first excited minimum MS2 at the point Q_2, when the values υ_1, υ_2 and t are non-vanishing. Such a minima conversion justifies to an extent the evaluation of the starting value of the parameter V with the aid of Eq. (8) and the experimental value of the activation energy for the MS2 state. However, the inclusion in the model of the interaction with the full-symmetric vibration A_1 (Fig. 2) and of the electron transfer processes brings to a lower value of the barrier height between the ground (GS) and first excited minima (MS2) as compared with experimental data (see Fig. 3). In Fig. 5(a) the energy gaps between the ground and excited minima as functions of the vibronic parameter V are reported. In Fig. 5(b) for the same values of the parameters the angles β_i describing the geometrical configurations of the Fe–(NO) moiety in these minima are quoted. When the vibronic parameter V falls inside the range $7 < V/\hbar\omega_{B_1} < 8.3$ the ground adiabatic potential sheet only possesses two minima. The ground minimum conforms with the bent configuration. In this case the angle $\beta_2 = \beta_1 = 75^\circ$ remains practically unchanged in the above mentioned range of the parameter V. The first excited minimum lies much higher than the ground one. Meanwhile, with the increase of the parameter V the energy gap between the two minima diminishes. The angle β_3 that relates to the excited minimum decreases slowly for $V < 8.3\hbar\omega_{B_1}$ and corresponds to a slightly kinked configuration in which the NO-ligand is O-bound to the iron ion. In the range $8.3 < V/\hbar\omega_{B_1} < 9.72$ the lower adiabatic potential sheet has three minima. However, in the ground minimum the geometrical structure of the Fe–NO moiety remains bent ($\beta_1 = 75^\circ$). The first excited minimum conforms to a kinked configuration with the N-bound NO fragment. The corresponding angle β_2 increases with the growth of the parameter V, and the moiety Fe–N–O begins to straighten. At the same time the angle β_3 characterizing the geometrical structure of the FeNO molecule in the highest adiabatic potential minimum tends to zero. Only in a small range of the vibronic parameter V values $9.72 < V/\hbar\omega_{B_1} < 9.85$ the configurations of the Fe–NO cluster in the minima of the ground adiabatic potential sheet conform to those observed for sodium nitroprusside [10]. If the parameter υ_1 characterizing the coupling of the $^1B_2$ state with the full-symmetric vibration varies and all other parameters are fixed (Fig. 6(a, b)) again only in a narrow range $0.95 < \upsilon_1/\hbar\omega_{B_1} < 1.63$ the situation resembles that in sodium nitroprusside. It is worth to note that changing the parameter υ_2 we also have found a single narrow range of its values allowing to interpret qualitatively the experimental data. As to the transfer integral (Fig. 7(a, b)) in comparison with other characteristic parameters a much wider range of its change ($t/\hbar\omega_{B_1} > 4.4$) provides

Table 1

Minimum	Q_i	q_i	Angle β (theory)	Angle β (experiment)
Ground	−9.63	−3.21	146	176
First excited	−0.21	−0.06	74.8	82
Second excited	9.83	−3.28	0.1	3

Angles (°) for the ground, first and second excited minima of the lower adiabatic potential sheet in the case of $V = 9.8\hbar\omega_{B_1}$, $t = 5.5\hbar\omega_{B_1}$, $\upsilon_2 = 6.2\hbar\omega_{B_1}$, $\upsilon_1 = 1.5\hbar\omega_{B_1}$, $\Delta_1 = 15\,850$ cm^{-1}, $\Delta_2 = 21\,185$ cm^{-1}, $\omega_{B_1} = 344$ cm^{-1}, $\omega_{A_1} = 403$ cm^{-1}.

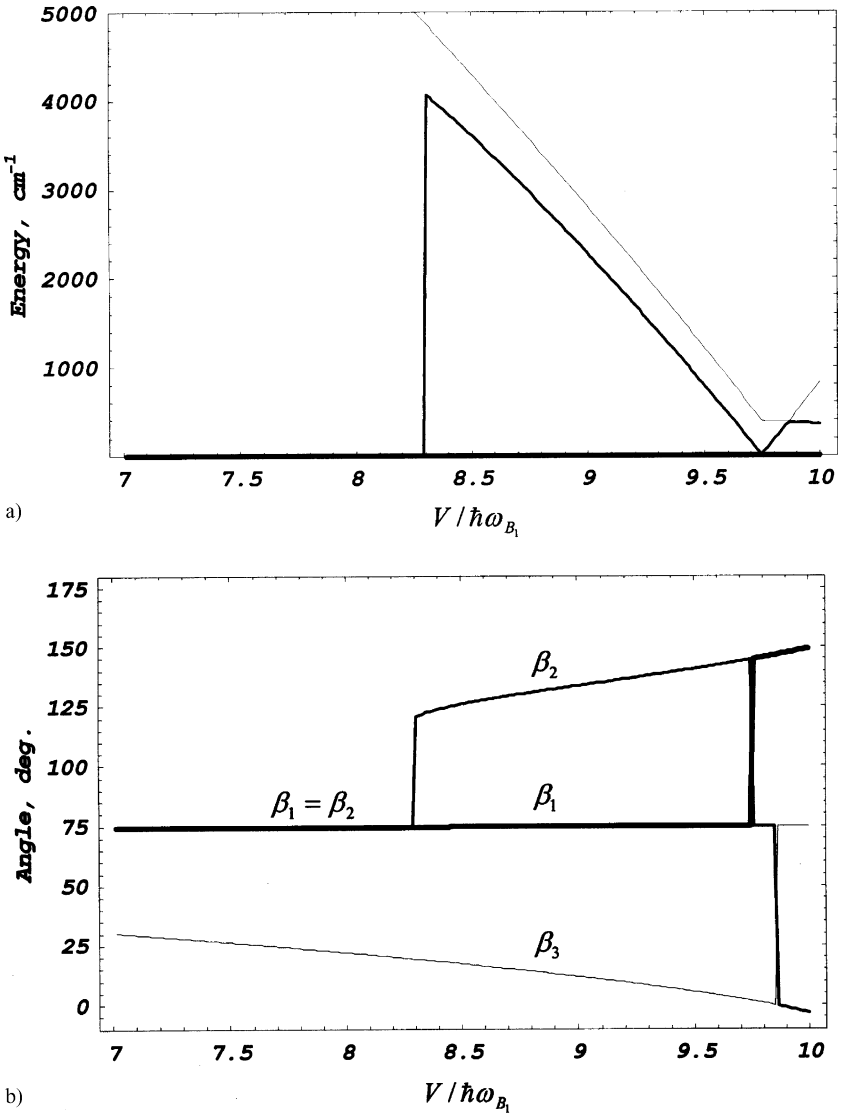

Fig. 5. Energy gaps (a) between the ground and excited minima of the lower adiabatic potential sheet $U_{gr}(q,Q)$ and angles β_i (b) characterizing the configuration of the Fe–(NO) fragment in these minima as functions of the vibronic parameter V with $t = 5.5\hbar\omega_{B_1}$, $\upsilon_2 = 6.2\hbar\omega_{B_1}$, $\upsilon_1 = 1.5\hbar\omega_{B_1}$, $\Delta_1 = 15\,850\ cm^{-1}$, $\Delta_2 = 21\,185\ cm^{-1}$, $\omega_{B_1} = 344\ cm^{-1}$, $\omega_{A_1} = 403\ cm^{-1}$. ▬▬—ground minimum, β_1; ——————energy gap between the first excited and ground minima, β_2; ——————energy gap between the second excited and ground minima, β_3.

the observed order of the increase of the energy from the GS to MS2 and MS1 states. For $t/\hbar\omega_{B_1} > 4.4$ the angles β_1, β_2, β_3 (Fig. 7(b)) corresponding to the states GS, MS1, MS2 as well as the energy gap between the states GS and MS2 remain practically unchanged (Fig. 7(a)). Simultaneously the energy gap between GS and MS1 states increases with the growth of the parameter t (Fig. 7(a)). At the same time the increase of the parameter t in the range ($t/\hbar\omega_{B_1} > 4.4$) leads to the decrease of the heights of the barriers between GS and MS2 or between MS2 and MS1. For instance, for $t = 5.5\hbar\omega_{B_1}$ the barrier height between GS and MS2 amounts to 0.3 eV, while for $t = 8\hbar\omega_{B_1}$ this height is equal to 0.2 eV. Survey of the Fig. 5(b)Fig. 6(b)Fig. 7(b) illustrating the influence of the parameters V, υ_1 and t on the angle $\angle$ FeNO (Fig. 2) leads to a conclusion that a range of these parameters can be indicated wherein the model reproduces the main experimental features of the photoexcited long-living metastable states in sodium nitroprusside and other transition-metal nitrosyl complexes [1–6]. In accordance with the experiment we have obtained that in the MS1 state the nitrosyl group is linked with the iron ion on the oxygen atom side, while in the MS2 state the coordination of nitrosyl is side-on. It should be noted that the study reported in this paper demonstrates the possibility of the existence of two metastable states that differ in energy and the corresponding configurations of the Fe–(NO) fragment. At the same time quantitative estima-

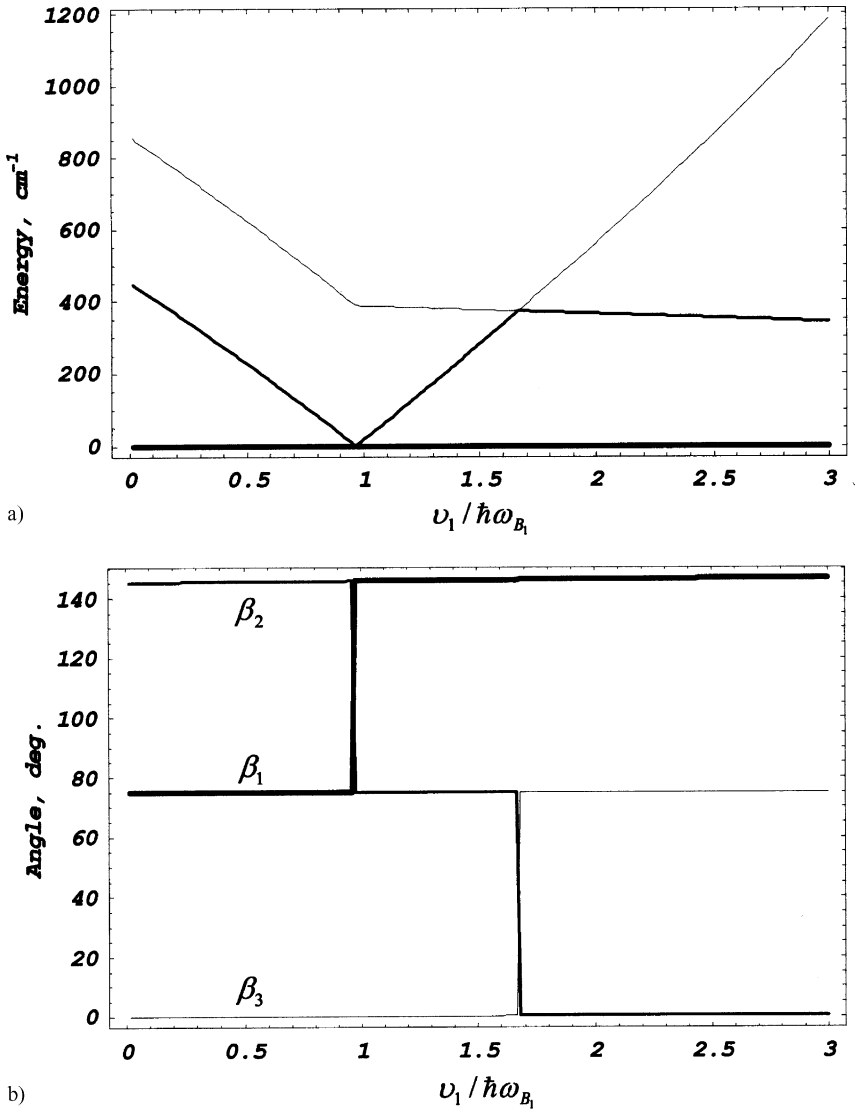

Fig. 6. Dependence of the energy gaps (a) between the ground and excited minima of the lower adiabatic potential sheet $U_{gr}(q,Q)$ and of the angles β_i (b) determining the configuration of the Fe–(NO) moiety in these minima on the vibronic parameter υ_1 with $V = 9.8\hbar\omega_{B_1}$, $t = 5.5\hbar\omega_{B_1}$, $\upsilon_2 = 6.2\hbar\omega_{B_1}$, $\Delta_1 = 15\,850$ cm^{-1}, $\Delta_2 = 21\,185$ cm^{-1}, $\omega_{B_1} = 344$ cm^{-1}, $\omega_{A_1} = 403$ cm^{-1}. ——ground minimum, β_1; ——energy gap between the first excited and ground minima, β_2; ——energy gap between the second excited and ground minima, β_3.

tion of the characteristic parameters for the Fe–(NO) cluster remains outside of our consideration. This problem needs special analysis in future.

4. Qualitative discussion. Concluding remarks

Below we briefly dwell upon the question of the heights of the barriers separating GS, MS1, MS2 states and the mechanism of population of the metastable states by photoexcitation. In Fig. 8 the three adiabatic potential surfaces obtained by diagonalization of the Hamiltonian (Eq. (5)) are reported. The first excited adiabatic potential sheet $U_1(q,Q)$ has two minima, the highest sheet $U_2(q,Q)$ is cone-shaped and possesses one minimum. The light induced Franck–Condon transition from the lowest minimum (GS) of the ground adiabatic potential sheet $U_{gr}(q,Q)$ to the sheet $U_2(q,Q)$ leads to the population of the single minimum of this sheet, then the relaxation can be followed by a radiative (or non-radiative) deexcitation onto the ground adiabatic potential surface populating thus with a significant probability the local minimum MS2. Another way of depopulation of the minimum of the branch $U_2(q,Q)$ passes through two minima of the middle adiabatic potential sheet $U_1(q,Q)$. In this case GS, MS2 and MS1 may be populated. The light-induced transition of the system from GS to the $U_1(q,Q)$-surface results in the population of the highest minimum of this surface. The decay of this excitation may lead to the population of GS and MS2. The optical transitions from MS1 and MS2 to $U_1(q,Q)$ have lower energies than that from GS

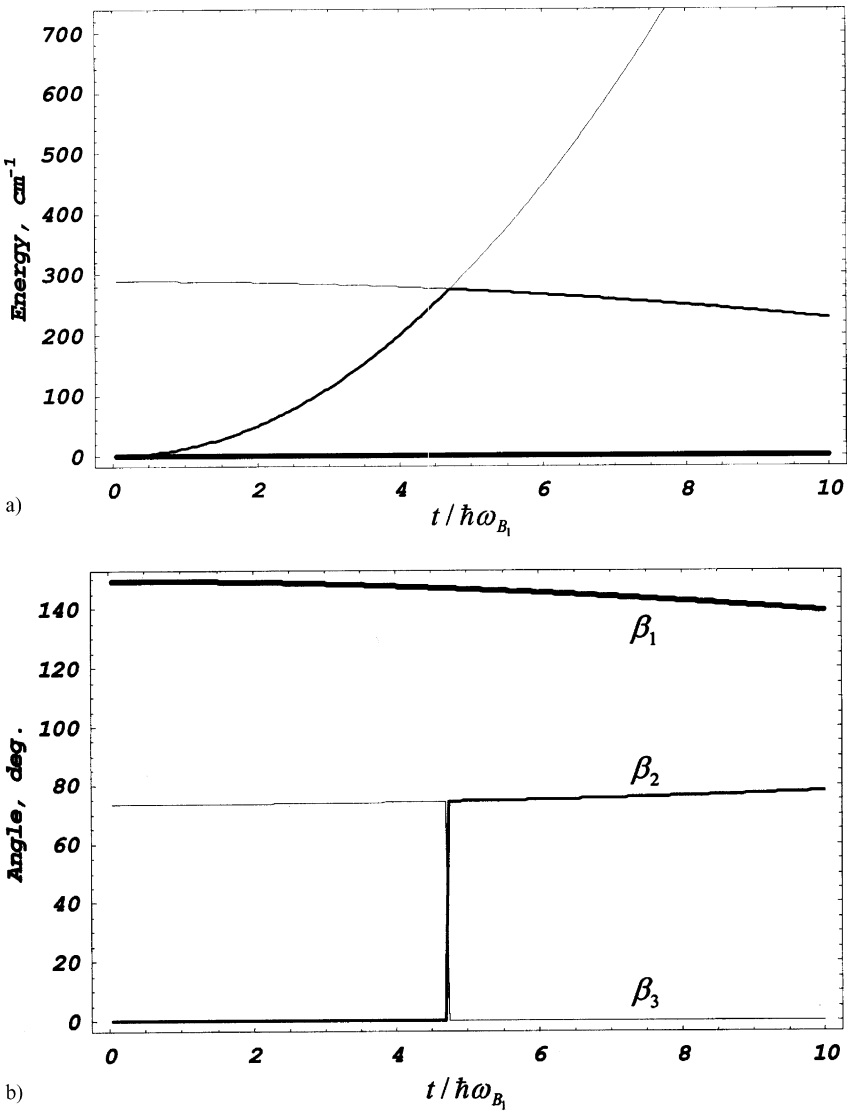

Fig. 7. Energy gaps (a) between the ground and excited minima of the lower adiabatic potential sheet $U_{gr}(q,Q)$ and angles β_i (b) characterizing the configuration of the Fe–(NO) fragment in these minima as functions of the transfer parameter t with $V = 9.8\hbar\omega_{B_1}$, $\upsilon_2 = 6.2\hbar\omega_{B_1}$, $\upsilon_1 = 1.5\hbar\omega_{B_1}$, $\Delta_1 = 15\,850\ cm^{-1}$, $\Delta_2 = 21\,185\ cm^{-1}$, $\omega_{B_1} = 344\ cm^{-1}$, $\omega_{A_1} = 403\ cm^{-1}$. ▬▬—ground minimum, β_1; ▬▬—energy gap between the first excited and ground minima, β_2; ▬▬—energy gap between the second excited and ground minima, β_3.

to $U_2(q,Q)$. However, the transition MS1 $\rightarrow U_1(q,Q)$ populates MS2, whereas the transition MS2 $\rightarrow U_1(q,Q)$, in its turn, transfers the system to MS1. In such a way, the carried out consideration shows that in the framework of the adiabatic potential scheme presented in Fig. 8 it is possible to go from GS into MS1 and MS2, from MS1 into MS2 and vise versa. The indicated ways of population of the metastable states on the basis of the obtained adiabatic potential scheme are in qualitative agreement with experimental data [8]. However, at this stage, the estimation of the wavelengths of the corresponding transitions seems to be premature.

As to the obtained values of the barrier heights they have the same order of magnitude as the experimental values of the activation energies for the metastable states MS1 and MS2 [8]. The obtained relation between the barrier heights (Fig. 3(b)) separating the GS-state and the metastable states seems to be also correct. At the same time the order of the minima of the ground potential sheet, the higher barrier between the MS1 and MS2 states along with the absence of a direct contact between the potential wells corresponding to GS and MS1 (Fig. 3(b) Fig. 4) allows us to make a conclusion that our model gives a decay temperature for the MS2 state lower than that of the MS1 state, and this is in agreement with experimental data [7,8]. In spite of the fact that the calculated barriers are smaller than the experimental values of the activation energies these barriers are sufficiently large to explain the long lifetimes of the MS1 and MS2 states.

Qualitative comparison of the theory with experiment shows that the employed model takes into account the

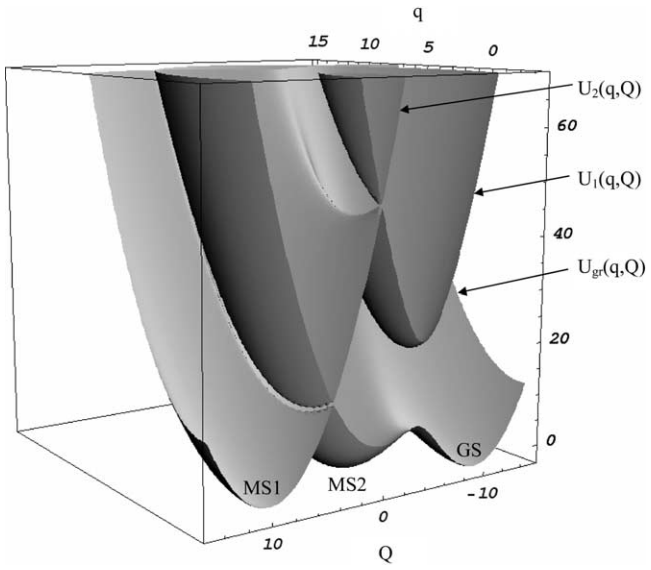

Fig. 8. The adiabatic potential sheets $U_{gr}(q,Q)$, $U_1(q,Q)$ and $U_2(q,Q)$ in the case of $V = 9.8\hbar\omega_{B_1}$, $t = 5.5\hbar\omega_{B_1}$, $\upsilon_2 = 6.2\hbar\omega_{B_1}$, $\upsilon_1 = 1.5\hbar\omega_{B_1}$, $\Delta_1 = 15\,850\ \mathrm{cm}^{-1}$, $\Delta_2 = 21\,185\ \mathrm{cm}^{-1}$, $\omega_{B_1} = 344\ \mathrm{cm}^{-1}$, $\omega_{A_1} = 403\ \mathrm{cm}^{-1}$.

main physical interactions responsible for the existence of long-living metastable states which differ in energy and geometrical configuration. These interactions are: vibronic coupling with the non-symmetric B_1-mode which bends the triangular fragment F–NO, vibronic coupling with the full-symmetric A_1-mode mode and tunnel interaction which provoke different barrier heights and different energies of the lower adiabatic potential sheet minima. However, for a more clear understanding of the nature of the metastable states it is necessary to solve the dynamic vibronic problem. The solution of this problem will give detailed information about the localization of the excitation in the minima of the lower adiabatic potential sheet. Not less important is the problem of quantum-mechanical calculation of the vibronic coupling constants and of the transfer parameter. Both these problems we are going to address to in future.

Acknowledgements

Financial support of INTAS (Project 2000-0651) and Supreme Council on Science and Technological Development of Moldova (grant 111) is highly appreciated. We thank Mihail Atanasov for the preprint of the paper [17] and fruitful discussion.

References

[1] (a) U. Hauser, V. Oestreich, H.D. Rohrweck, Z. Phys. A280 (1977) 17;
(b) U. Hauser, V. Oestreich, H.D. Rohrweck, Z. Phys. A280 (1977) 125.
[2] U. Hauser, V. Oestreich, H.D. Rohrweck, Z. Phys. A284 (1978) 9.
[3] T. Woike, H. Zöllner, W. Krasser, S. Haussühl, Solid State Commun. 73 (1990) 149.
[4] T. Woike, S. Haussühl, Solid State Commun. 86 (1993) 333.
[5] J.A. Güida, O.E. Piro, P.J. Aymonino, Inorg. Chem. 34 (1995) 4113.
[6] K. Ookubo, Y. Morioka, H. Tomizawa, E. Miki, J. Mol. Struct. 379 (1996) 241.
[7] H. Zöllner, T. Woike, W. Krasser, S. Haussühl, Z. Kristallogr. 188 (1989) 139.
[8] T. Woike, W. Kirchner, G. Schetter, T. Barthel, K. Hyung-Sang, S.S. Haussühl, Opt. Commun. 106 (1994) 6.
[9] M.R. Pressprich, M.A. White, Y. Vekhter, P. Coppens, J. Am. Chem. Soc. 116 (1994) 5233.
[10] M.D. Carducci, M.R. Pressprich, P. Coppens, J. Am. Chem. Soc. 119 (1997) 2669.
[11] H. Zöllner, W. Krasser, T. Woike, S. Haussühl, Hyperfine Interact. 7 (1993) 265.
[12] C. Terrile, O.R. Nascimento, I.J. Moraes, E.E. Castellano, O.E. Piro, J.A. Guida, P.J. Aymonino, Solid State Commun. 73 (1990) 481.
[13] J.A. Guida, O.E. Piro, P.J. Aymonino, Solid State Commun. 57 (1986) 175.
[14] B. Delley, J. Scheffer, T. Woike, J. Chem. Phys. 107 (1997) 10067.
[15] P. Boulet, M. Buchs, H. Chermette, C. Daul, F. Gilardoni, F. Rougemond, C.W. Schläpfer, J. Weber, J. Phys. Chem. A105 (2001) 8991.
[16] P. Boulet, M. Buchs, H. Chermette, C. Daul, F. Gilardoni, F. Rougemond, C.W. Schläpfer, J. Weber, J. Phys. Chem. A105 (2001) 8999.
[17] M. Atanasov, T. Schönherr, TheoChem, 2002, in press.
[18] Y.E. Perlin, B.S. Tsukerblat, Effects of Electron-Vibrational Interaction in the Optical Spectra of Paramagnetic Impurity Ions, Shtiintsa, Kishinev, 1974, p. 368.
[19] L.D. Landau, E.M. Lifshits, Mechanics, Nauka, Moscow, 1965, p. 203.
[20] J.P. Elliot, P.G. Dawler, Symmetry in Physics, Principles and Simple Applications, vol. 1, The Macmillan Press Ltd, London, 1979, p. 364.